J. Physiol. (1980), **299**, *pp.* 573–603
With 16 *text-figures*
Printed in Great Britain

RELATIONS BETWEEN THE INACTIVATION OF SODIUM CHANNELS AND THE IMMOBILIZATION OF GATING CHARGE IN FROG MYELINATED NERVE

BY W. NONNER

From the Physiologisches Institut der Universität des Saarlandes, 6650 Homburg/Saar, Federal Republic of Germany and the Department of Physiology and Biophysics, University of Washington School of Medicine, Seattle, Washington 98195, U.S.A.*

(*Received 27 March 1979*)

SUMMARY

1. Single, voltage-clamped nerve fibres of *Rana esculenta* were stimulated with 'P/2' pulse patterns for measuring Na and gating currents at 13 °C.

2. Gating currents during test pulses to −122 or +10 mV were measured after 45 msec conditioning steps to voltages between −122 and −18 mV. As the conditioning voltage was made more positive than −80 mV, the movable gating charge diminished along a sigmoid curve, approaching a value of nearly one third of the maximum charge. On the other hand, Na inactivation began at a more negative potential and proceeded to undetectable levels.

3. After a depolarizing prepulse, both time constant and size of the charge movement depended less steeply on the test voltage than normally. The prepulse reduced gating currents associated with steps from −122 to test voltages $\geqslant -40$ mV, but enhanced gating currents obtained with test voltages < -40 mV.

4. Increasing the duration of a depolarizing pulse (−54 to +42 mV) reduced the fast 'off' gating current at the end of the pulse and enhanced a slow component. Their total charge corresponded approximately to that carried during the pulse. During depolarization, Na current inactivated in a fast and a slow phase. The fast phase was also reflected in the loss of fast charge movement (immobilization) as seen after the pulse was interrupted at various durations.

5. The available Na current and the fast movement of gating charge diminished in parallel during prepulses more positive than −54 mV, and recovered in parallel upon repolarization to levels between −102 and −46 mV. During prepulses between −62 and −78 mV, however, Na inactivation occurred up to 4 times faster than charge immobilization. Also, at −78 mV, Na current was inactivated 3 times faster than it recovered.

6. These findings indicate that Na inactivation and charge immobilization are linked, but proceed with high-order kinetics. The simplest scheme that accounts for their relation is

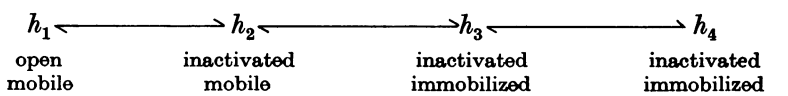

* Where experiments were done.

0022-3751/80/6680-0116 $07.50

Depending on voltage, either state h_2 ($E > -45$ mV) or h_3 ($E < -45$ mV) becomes kinetically undetectable.

7. A model of the Na channel is developed in which inactivation gains most of its voltage dependence by a coupling to the fast charge movement (activation). The model is shown to be quantitatively consistent with the results. In particular, the change of kinetics observed near -45 mV can be explained as an effect of the redistribution of charges on the inactivation process.

INTRODUCTION

The Na channels of nerve membranes open quickly upon a depolarization and also close quickly upon a repolarization. Conducting channels close and non-conducting channels become unavailable for opening during a longer depolarization, and they recover after the depolarization. These kinetic events have been described successfully in terms of two mutually independent gating processes: activation and inactivation (Hodgkin & Huxley, 1952). Indeed, as reviewed by Meves (1978), various toxins, venoms, chemical agents, and enzymes modify inactivation without much effect on activation, or vice versa. On the other hand, the channels must bear an electrical charge or dipole moment in order to achieve the steep dependence on membrane voltage characteristic for these gating processes. Even if two separate sets of charges or dipoles existed in each channel, some electrostatic interaction would be likely.

In recent years, a component of membrane capacity current has been investigated that is thought to originate from rearrangements of gating charges, or dipoles, in Na channels (for reviews see Meves, 1978; Almers, 1978; Neumcke, Nonner & Stämpfli, 1978). A depolarization of several milli-seconds reversibly reduces the size of this gating current as has been shown in squid axons (Armstrong & Bezanilla, 1977; Meves & Vogel, 1977) and in myelinated nerve (Nonner, Rojas & Stämpfli, 1978). The phenomenon has been called 'immobilization' or 'inactivation' of gating charge, and has in two recent studies on squid axons been compared to the inactivation of Na current. Armstrong & Bezanilla (1977) concluded that immobilization and Na inactivation were due to one and the same event, whereas Meves & Vogel (1977) suggested an indirect relation between both phenomena.

The first part of this paper describes experiments on myelinated nerve in which immobilization and Na inactivation are compared for the same nodes of Ranvier. Na inactivation is found to reveal kinetics of high order, as already described by Chiu (1977). Under depolarization (when Na channels are activated), immobilization appears to reflect the closing of the channels by inactivation, whereas at rest or more negative voltages (where Na channels are not activated), immobilization seems to reflect another step of the inactivation mechanism. The second part of the paper presents a quantitative model in which these findings are interpreted in terms of an interaction between activation and inactivation. A part of the results has been presented at a meeting of the Biophysical Society (Nonner, 1979).

PART I: EXPERIMENTS

METHODS

Protocol

Single myelinated nerve fibres of the frog (*Rana esculenta*) were studied with a voltage-clamp technique (Nonner, 1969) at 13 °C. A computer generated command pulses ('P/2' pattern), recorded and averaged samples of membrane current (1–64 sweeps), and stored them on digital magnetic tape. As a rule, first Na and then gating currents were measured in the same nerve

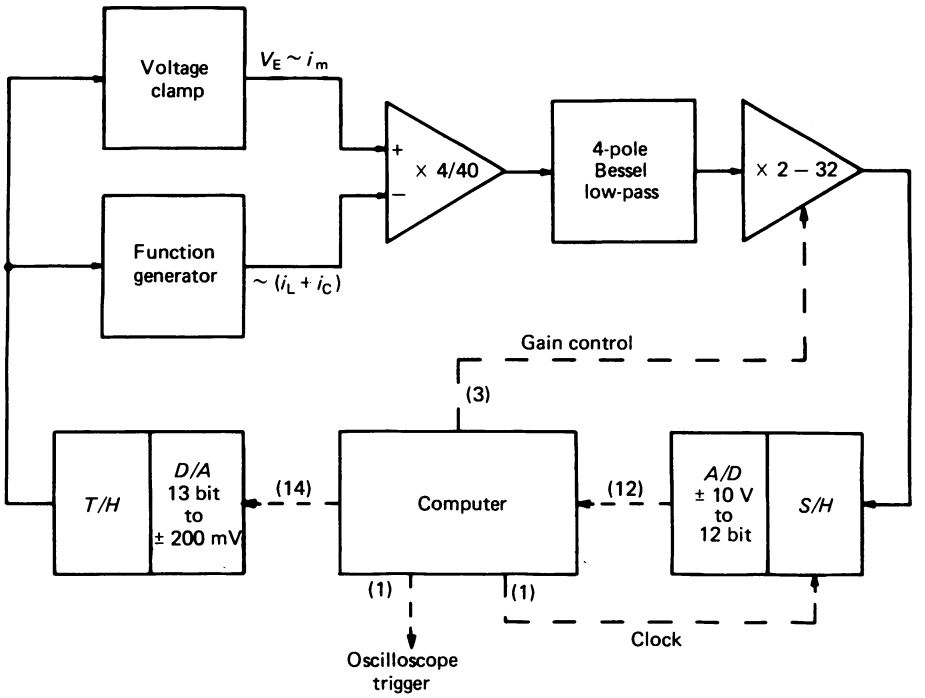

Fig. 1. Schematic diagram of recording apparatus. The digital computer (DDP-516, Honeywell–Bull) has a word length of 16 bit and a 16 k, 0·96 μsec memory. It controls the other equipment via digital lines (dashed, number in parentheses). The *D/A* converter is an AN 1912 (Analogics), the transient-suppressing track-and-hold circuit a MP259 (Analogics). The function generator produces the sum of three exponentially declining and a constant voltage, all proportional to the commanded voltage. Time constants and amplitudes can be varied by hand. Amplifiers are homemade devices containing fast-settling operational amplifiers (HA-2525) and, for changing gain, field-effect transistor switches (DG 201, Siliconix). The low-pass filter is a FC-104-4 (Frequency Devices). The sample-and-hold (*S/H*) circuit and *A/D*-converter are part of a MP 6912 module (Analogics).

fibre and with the same pulse programme. First, Na current was recorded in the presence of 6 nM-external tetrodotoxin (TTX); at this concentration, the toxin blocked about three quarters of the Na channels and, thus, reduced artifacts due to a series resistance. Then, the node was perfused with an external solution containing tetramethylammonium (TMA) ion in place of Na^+ and 300 nM-TTX, and gating currents were measured (substitution of Na^+ was necessary since there was a residual ionic current (up to about 100 pA) through Na channels not blocked by 300 nM-TTX). Throughout, K current was eliminated by 10 mM-external tetraethylammonium (TEA) ion and by an artificial 'axoplasm' containing Cs^+ in place of K^+. Between

sweeps, the membrane voltage was held at −98 mV. Membrane currents were calibrated from the dimensions of the fibre as measured at the end of the experiment (Conti, Hille, Neumcke, Nonner & Stämpfli, 1976). Internodal diameters varied between 15·1 and 18·9 μm.

Stimulating and recording

Fig. 1 shows a block diagram of the apparatus. A computer generated the command voltage through a digital-to-analogue converter (D/A) at a resolution of 13 bits. The voltage was fed through a track-and-hold circuit (T/H, which suppressed switching transients of the converter) to the voltage-clamp circuit and to a function generator. The generator produced a signal that

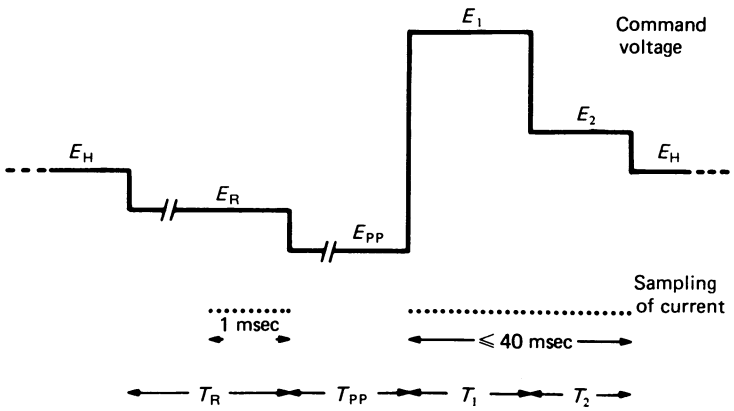

Fig. 2. Time diagram of a sweep. Samples are taken at 10·2 μsec intervals.

could be adjusted to correspond approximately to the leak and capacity currents during a negative pulse. This signal, $i_L + i_C$, was subtracted from the membrane-current signal, i_m, before further amplification. After a first amplifier, which was set at a gain of 4 (Na current) or 40 (gating current), the difference signal was low-pass filtered and fed through a second amplifier, the gain of which was varied in powers of 2 under control of the computer. For each pulse pattern, the computer first recorded one sweep at the lowest gain, calculated the maximum useful gain, and, after switching the amplifier to this gain, recorded the sweeps to be saved. The final current signal was sampled at 10·2 μsec intervals and converted into 12-bit digital samples.

The approximate subtraction of linear components of membrane current by the analogue circuit was made exact by a digital procedure. Currents during each test sweep for the pulse sequence to be studied were added together with the (inversed) currents from two control sweeps. The control pulses had half the size of the test pulses, were applied from voltages between −98 and −122 mV, and their direction was normally opposite to that of the test pulses. Fig. 2 shows the most general sequence of pulses during a sweep. From the holding level, E_H, up to four subsequent pulses were applied: a pulse to a 'reference' voltage, E_R (at which the baseline of the current was recorded), a prepulse to E_{PP}, and two test pulses to E_1 and E_2. In many experiments, reference and prepulse were to the same voltage ($E_{PP} = E_R$), or only one test pulse was used ($E_2 = E_R$). Control sweeps were taken with a hyperpolarizing reference pulse and with the other pulse levels adjusted to fulfil the relation

$$\frac{E'_X - E'_R}{E''_X - E''_R} = -K \; (E_X = E_{PP}, E_1, E_2), \tag{1}$$

where single primes indicate voltages of the test sweep, and double primes those of the control sweeps. K was normally 2 or, in a few experiments, −2; this relation was automatically maintained by the computer program.

The current was sampled at 10·2 μsec intervals during the last millisecond of the reference pulse and during both test pulses; the combined length of the two test pulses could be varied from 0 to 40 msec. The 100 base-line samples were averaged into one value to be stored. The

other samples (up to 4000) were, for each test pulse, divided into one fixed section (the first 0·5 msec), where all samples were stored, and two sections of variable length, during which each n, or n^2, subsequent samples were averaged together. The number n was chosen by the program such that about twenty-five condensed samples resulted from each of the second and third sections. Thus, a record of up to 4100 samples was condensed into a maximum of 201 stored samples.

Sweeps and control sweeps were averaged in separate buffers of condensed samples. For

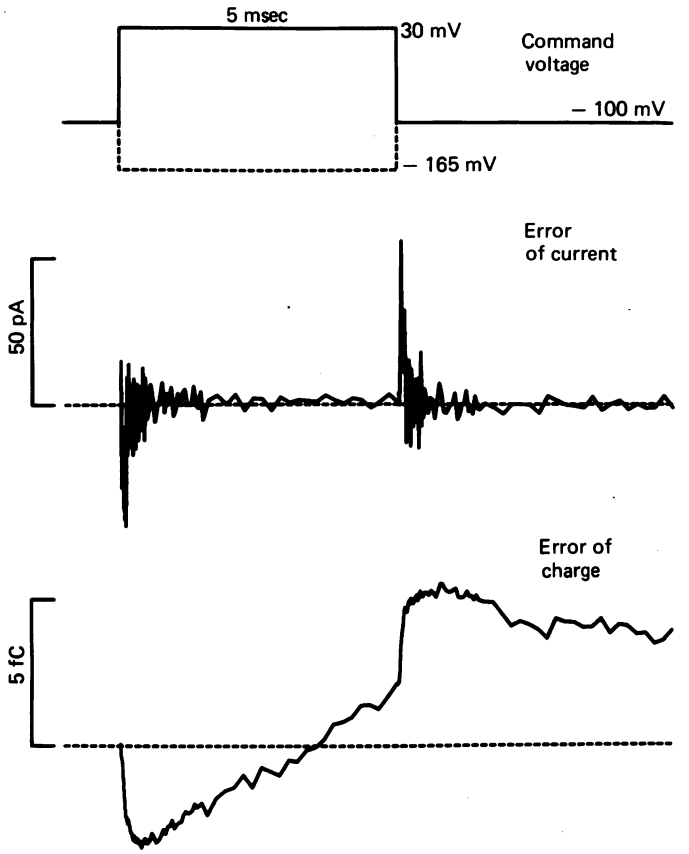

Fig. 3. Error of current (middle) and charge measurement (bottom) with a nerve model. The pulse programme of Fig. 2 was simplified by choosing $E'_2 = E'_{PP} = E'_R = E''_R = E_H = -100$ mV. T_1 and T_2 were 5 msec. Sixty-four triplets of sweeps were taken at a gain of 32 in the second amplifier (Fig. 1), and averaged. The variation of noise with time is due to the condensing of samples beginning at 0·5 msec after each change of voltage.

measuring Na current, 1–16 triplets of sweeps and control sweeps were averaged at an interval of 1 sec between sweeps. For gating currents, 64 triplets were taken at sweep intervals of 0·5 sec.

The recording apparatus was tested with a model circuit representing the nerve fibre and external resistances. Fig. 3 gives an example, in which a large test pulse was used and the second amplifier was operating at the highest gain. The traces represent the error of the net current (middle) and net movement of charge (bottom, numerical integral of middle trace). These errors may be compared to the gating current of 1–2 nA or a gating charge of 100–150 fC that would be obtained from a nerve fibre. At a lower gain, the dynamic error was about equally large (and mainly reflected a common-mode error of the $(i_L + i_C)$-subtractor), whereas the static error

diminished with the gain (and represented mainly a linearity error of the A/D-converter). Most of the gating currents were measured at gains of 16 or 32 in the final amplifier.

Curve fitting procedures

When theoretical expressions were fitted to time courses of currents or charges, parameters were found in two steps. The measured points were transformed to yield straight lines or curve segments and analysed by linear regression. The parameters from this procedure were further improved by repeated non-linear regression, on the original points, with the least-squares method of Gauss. This algorithm also provided estimates of standard deviations for the parameters, which indicated both the goodness of a fit as well as the limits that could be imposed on a particular parameter.

Solutions

The cut ends of the nerve fibre were bathed in an 'axoplasm' solution containing 120 mM-CsCl. Na current was measured with the node of Ranvier in the following external solution: 110·5 mM-NaCl, 2 mM-$CaCl_2$, 2 mM-N-morpholino-3-propane-sulphonic acid (MOPS)-NaOH buffer (pH = 7·4), 10 mM-TEACl, 6 nM-TTX. During measurements of gating current, the external solution contained 110·5 mM-TMACl, 2 mM-$CaCl_2$, 2 mM-MOPS-TMAOH buffer (pH = 7·4), 10 mM-TEACl, 300 nM-TTX. A change in the diffusion potential at the external electrode that acompanied a change between these external solutions (about 3 mV) was compensated by readjusting the holding potential.

Conventions

The voltage clamp was balanced to give a resting inactivation of Na channels equivalent to $h_\infty \simeq 0{\cdot}7$ as measured with a 60 mV depolarising pulse and with the node in ordinary Ringer solution. The absolute membrane potential, E, was assumed to equal -70 mV at this balance point. Outward membrane current is given as positive. Gating charges are measured in units of fC (10^{-15} A sec).

RESULTS

A conditioning voltage pulse alters the gating current of a node of Ranvier. Fig. 4 shows a pulse program and records taken for three conditioning voltages. The gating current was first measured while about three quarters of the Na current was blocked (lower traces), and, again, after Na current had been completely blocked (upper traces, plotted at a larger scale). Increasing the conditioning voltage from -122 to -74 or -34 mV inactivated Na current to about 60 % or zero. Gating current was slightly reduced by the prepulse to -74 mV, and was strongly reduced, but not abolished, at -34 mV. It declined more rapidly as the voltage of the prepulse increased. To the extent that gating current can be distinguished from Na current in the lower traces, it is altered in the same way as in the upper traces, where Na current is absent.

Apparently, the prepulse changes the size of Na and gating currents in the same direction, but to different degrees; it also modifies the time course of gating current. Before the comparison is continued, the alterations of the gating current are investigagated in more detail. For reasons given later, quantitative analysis is confined to a fast component of gating current that predominates in Fig. 4.

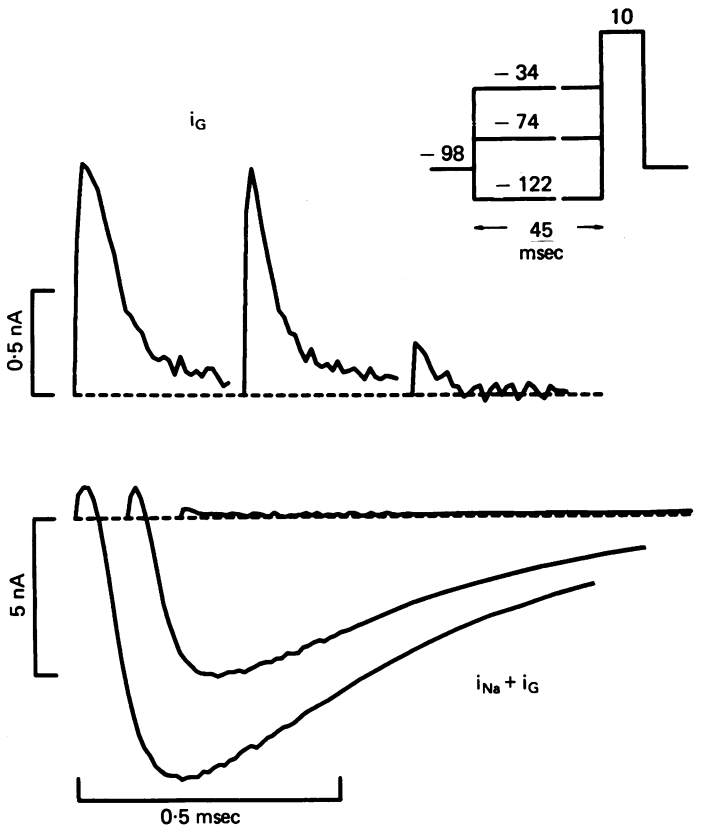

Fig. 4. Na and gating currents after different prepulses. Lower records ($i_{Na} + i_G$), taken with node in Ringer plus 6 nM-TTX, represent sums of gating current (positive transient) and Na current (negative wave, reaching about one quarter of normal size because of partial block by TTX). Upper records, taken later with node in TMA-Ringer plus 300 nM-TTX, reveal gating current alone (i_G, note larger scale). The traces refer to prepulses of -122, -74, and -34 mV (left to right). Inset shows E_H, E'_R, and E'_1 in mV; control pulses (not shown) were from $E''_R = -122$ mV, and with E''_1 according to eqn. (1), $K = 2$. Fibre 23/77; 13 °C; internal solution: 120 mM-CsCl.

Size of the mobile charge

The nodal gating current carries a saturable amount of charge, as if it were due to a finite number of electrical charges or dipoles rearranging within the membrane (Nonner *et al.* 1975). The effect of the prepulse on the total amount of movable charge was examined with the pulse programme shown in Fig. 5*A*. After each prepulse, the gating current was measured with a test pulse to +10 mV, and, again, with a test pulse to -122 mV. The records were corrected for a slow component of gating current, as described in the legend of Fig. 5, and integrated with respect to time, yielding the transfer of charge (Fig. 5*A*, traces). The quantities of charge moved during the first 0·3 msec of the positive and the negative test pulse were added together, and their sum was taken as a measure for the amount of mobile charge. In Fig. 5*B*, the results

from two experiments (symbols) and their mean (line) have been plotted *vs.* the conditioning voltage. Increasing the voltage of the prepulse above −80 mV reduces the mobile charge along a sigmoid curve that is steepest near the resting potential, −70 mV, and approaches a limit at strong depolarizations of about one third of the charge available with the largest hyperpolarization.

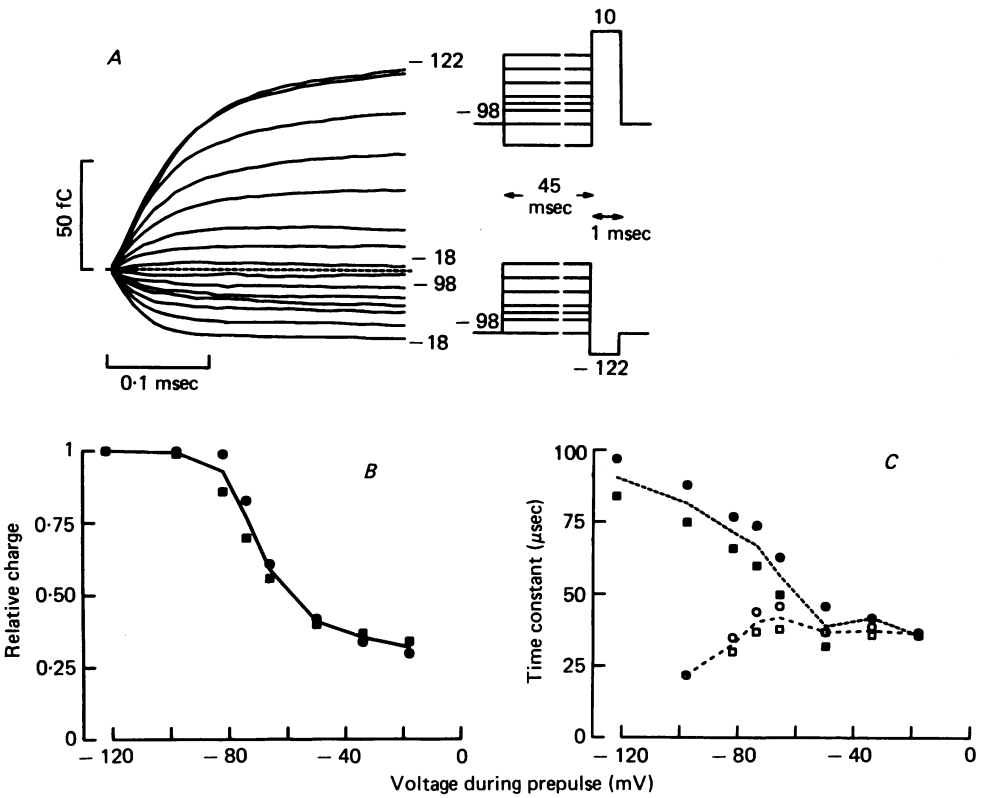

Fig. 5. Effects of prepulse voltage on fast charge movement. *A*, integrals of fast gating currents during test pulses to +10 mV (positive traces) or −122 mV (negative traces). Prepulses to −122, −98, −82, −74, −66, −50, −34, −18 mV (E'_R). Control pulses according to eqn. (1) with $K = 2$ (positive test pulses) or $K = -2$ (negative test pulses); E''_R was −122 mV throughout. Slow gating current was corrected for by subtracting mean current between 0·5 and 1 msec (positive test pulses) or 0·3 and 0·7 msec (negative test pulses) from rest of record before numerical integration. Fibre 24/77; 13 °C. *B*, size of mobile charge *versus* voltage of prepulse. Charges calculated by adding together the charges carried during the first 0·3 msec of each positive and negative test pulse. From traces *A*, ●, and another experiment (23/77), ■; means represented by line. *C*, time constants of fast charge movement versus voltage of prepulse. Filled symbols refer to positive, open symbols to negative test pulse. Experiments as in *B*; means indicated by lines.

Time course of charge movement

The effect of the prepulse on the time course of gating current, which was already seen in Fig. 4, was analysed by fitting integrated records as in Fig. 5*A* by

$$Q(t) = Q(\infty)\,(1-\exp[-t/\tau]).$$

In Fig. 5*C*, time constants, τ, from two experiments have been plotted *vs.* the voltage of the prepulse. The filled symbols refer to the positive test pulses and open symbols to the negative. After hyperpolarization, the charge movement settles about three

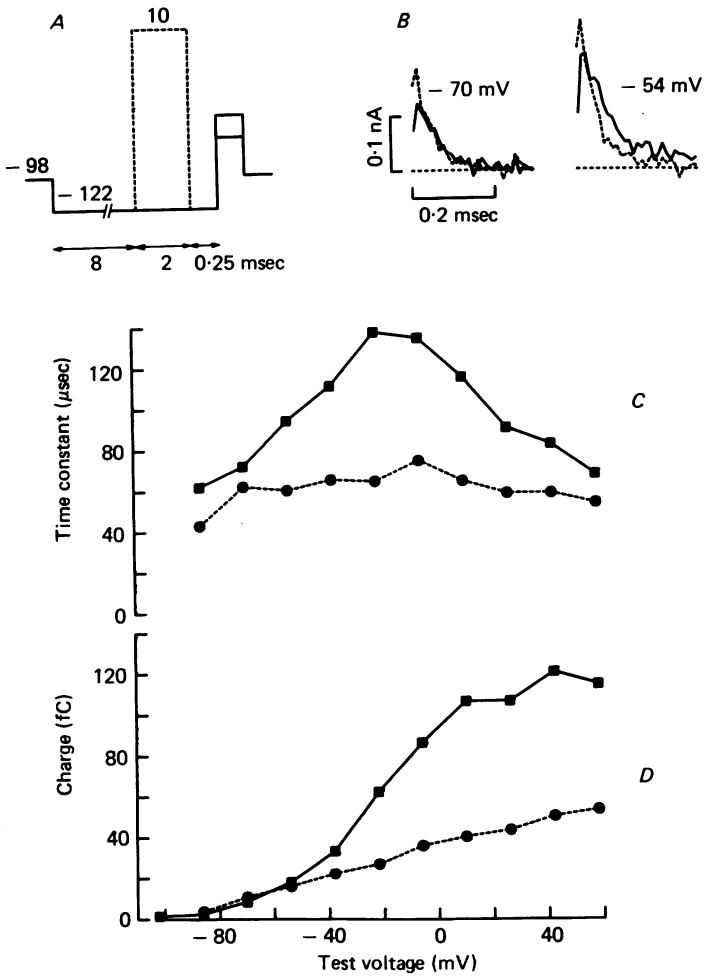

Fig. 6. Effect of a depolarizing prepulse on the voltage dependence of fast charge movement. *A*, pulse programme including, or not, a prepulse (E'_{PP}) to +10 mV, followed by an 0·25 msec interval at −122 mV (E'_1), and a test pulse (E'_2) to various levels (control pulses, not shown, according to eqn. (1) with $E''_R = -122$ mV, $K = 2$). *B*, gating currents without (continuous lines) or with the prepulse (dashed lines) at two voltages. Charges (*D*) and time constants (*C*), from these and other records, were calculated as for Fig. 5 and plotted *vs.* test voltage (■——■: without prepulse; ●- - -●: with prepulse). Fibre 3/78; 13 °C.

times faster during the negative than during the positive test pulse, whereas, after depolarization, the time courses are similar. Apparently, conditioning of the membrane emphasizes different kinds of charge movements, one with strongly voltage-dependent kinetics, which prevails after a hyperpolarization, and one with less voltage-dependent kinetics, which prevails after a depolarization.

This point was further examined with the pulse programme in Fig. 6*A*. The voltage of the test pulse was varied between −102 and +58 mV, and the gating current was measured without and, again, with a 2 msec prepulse to +10 mV. Time constants were calculated as before, and plotted *vs.* the voltage of the test pulse (Fig. 6*C*). Without the preceding depolarization (continuous line), the time constant depends, indeed, more strongly on the test voltage than after the depolarization (dashed line).

Steady-state distribution of charge

The charges carried by the gating currents of the same experiment are shown in Fig. 6*D* as a function of the test voltage. After the depolarizing prepulse (dashed line), the charge varied less steeply with voltage than after the hyperpolarization (continuous line), as if the voltage dependence of its steady-state distribution were reduced, like that of the kinetics (Fig. 6*C*).

Alterations of the voltage and time characteristics may be expected for quite different mechanisms of charge immobilization. Thus, depolarization may totally block charge movements in some structures, making it possible to observe a smaller contribution from other structures that are not blocked. On the other hand, depolarization may modify the transitions between states of the same charged structures. An indication for a mechanism of the second kind can be found in Fig. 6*D*. The Figure shows that the effect of the prepulse on the size of the charge changed with the voltage of the test pulse. A reduction was found with test voltages $\geqslant -40$ mV. No effect, or even a slight increase, was detected with a more negative test voltage. Fig. 6*B* presents the gating currents measured with the test pulses of −70 or −54 mV. The early current was larger with the depolarizing prepulse (dashed lines) than without (continuous lines). Results as in Fig. 6 were obtained in two other experiments. They suggest that the conditioning depolarization enables charges or dipoles to move along a different route that does not exist in a previously hyperpolarized membrane. The observations of Fig. 6*B*, *D* were close to the limits of resolution and were, therefore, re-examined with another pulse programme. This programme (Fig. 7, upper part) avoided the interval between conditioning and measurement, during which the after-effect of the prepulse may have been partially reversed.

Different test voltages were applied immediately after a prepulse to −122 or +42 mV. The integrals of the gating current, including the slow component, are shown in the middle of Fig. 7. The slow displacement of charge was particularly marked in the traces recorded after the depolarizing prepulse, a phenomenon to be considered later. The fast displacement of charge was separated by fitting a straight line between 0·5 and 1 msec (left traces) or 0·25 and 0·5 msec (right traces) and extrapolating to the charge at zero time. In the bottom of Fig. 7, the results for the hyperpolarizing prepulse, from this and another experiment, have been plotted against the test voltage (crosses, mean as continuous line). These points indicate how much charge was moved by stepping the voltage from −122 mV to a more positive level. For the depolarizing prepulse (filled symbols), the ordinate plots the charge movement on repolarization minus the charge movement measured on repolarization to −122 mV. These charge *vs.* voltage curves confirm the observation of Fig. 6: besides an immobilizing effect on part of the charge, a depolarizing prepulse *recruits* another kind of charge movement, preferably observed at voltages near the resting potential.

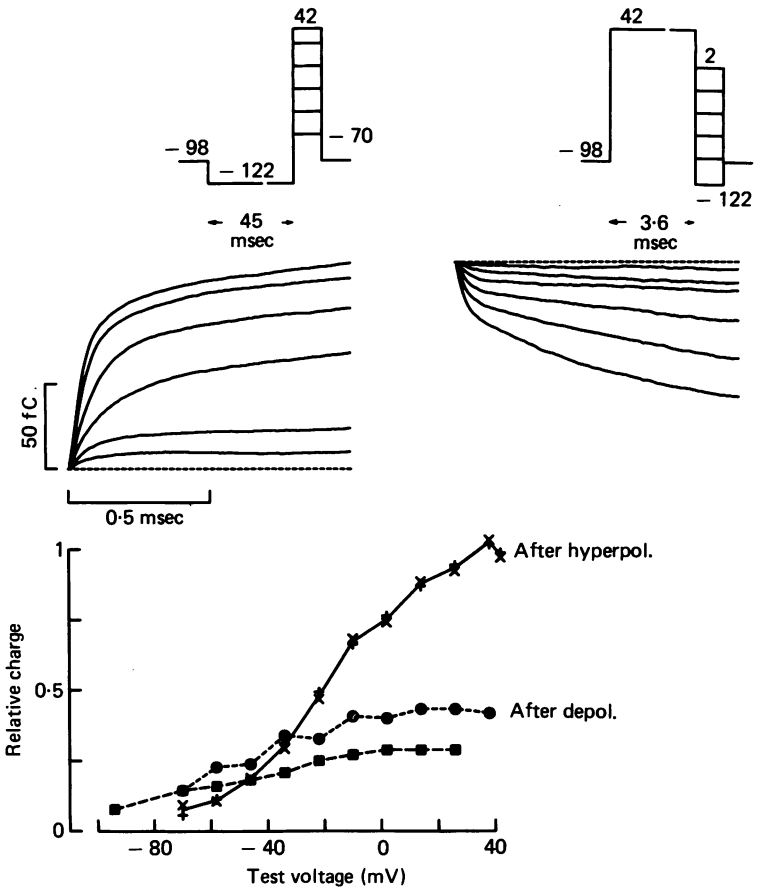

Fig. 7. Effect of prepulses on the voltage dependence of fast charge displacement (second method). Top: pulse programmes for hyperpolarizing (left) and depolarizing (right) prepulse (E'_R); test voltages (E'_1) were −70, −46, −22, −2, 26, 42 mV (left) or −122, −94, −70, −46, −22, 2 mV (right); control pulses, not shown, according to eqn. (1) with $E''_R = -122$ mV, $K = 2$. Middle: integrals of *total* gating currents during test pulses. Fibre 28/77; 13 °C. Bottom: charges displaced *vs.* voltage (for details see text), from the same and another fibre (27/77). Symbols + (27/77) and × (28/77) refer to hyperpolarizing prepulse (mean as continuous line), curves ●---● (27/77) and ■---■ (28/77) to depolarizing prepulse. Charges were normalized to 143 fC (27/77) or 103·5 fC (28/77).

Slow gating current

The immobilization of gating charge, as will be described later, developed and reversed in milliseconds. When part of the charge was immobilized during a depolarizing pulse, repolarization ought to produce, besides a rapid return of mobile charge, a slow movement within milliseconds of charge returning from immobilization. The two contributions should add up to the charge displaced during the pulse. This balance of charges was examined with a test pulse of variable duration, yielding different degrees of immobilization (Fig. 8). The gating current was integrated during the pulse and the subsequent 5 msec. Continuous traces represent the forward, and

dashed traces the reverse, movement of charge. After a short pulse, the entire charge returned quickly; after a longer pulse, only part returned quickly, and a remainder slowly. The growth of the slow phase approximately compensated for the loss in the fast phase as the pulse length was increased, so charge balance was roughly obeyed.

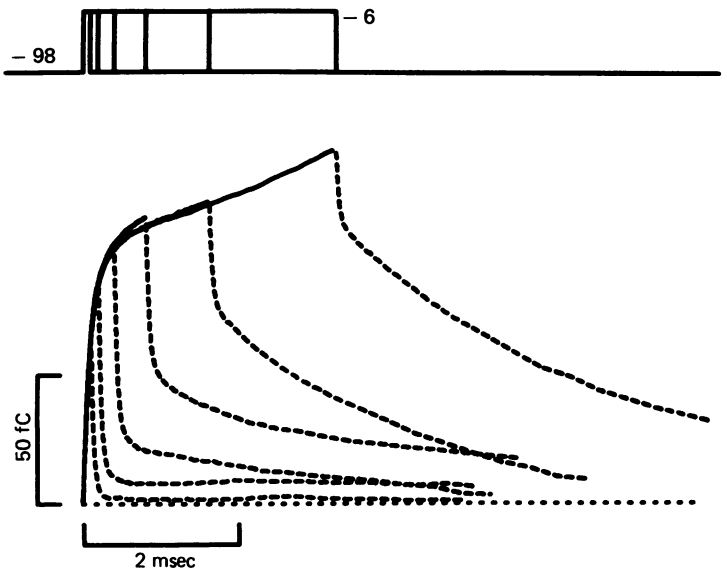

Fig. 8. Effect of pulse duration on the reverse charge movement. Integrals of *total* gating current during test pulse (solid lines) and subsequent 5 msec (dashed lines); superimposed traces for various pulse lengths as shown by inset (control pulses, not shown, according to eqn. (1) with $E_R'' = -98$ mV, $K = 2$). Fibre 6/78; 13 °C.

A slow component of gating current was regularly observed. It was outward with positive, and inward with negative, voltage steps as expected for a displacement current. Observations of slow *inward* currents made with positive voltage steps were always traced to a nascent anodal break-down of the membrane due to the large, negative control pulses. However, the slow gating currents revealed a larger variability than expected from control measurements on a nerve model, indicating that resolution was limited by properties of the nerve fibre. Deviations from charge balance as in Fig. 8 would be expected if the unblocked leakage current of several nanoamperes, and after-effects of such currents on the current base line (Nonner *et al.* 1978), were not linear and reproducible within about 1 pA. In the worst case, the error in the gating current could then be 3 times larger and contribute a charge error of 15–24 fC during an integration period of 5–8 msec. Therefore, quantitative analysis was confined to the fast gating current.

The next sections compare the immobilization of fast gating charge to the inactivation of ionic Na current as measured in the same nerve fibres. They also describe the time course of charge immobilization.

Charge immobilization and steady-state inactivation

Steady-state inactivation was determined from Na peak currents recorded during a test pulse to +10 mV, which followed a 45 msec conditioning pulse. Normalizing with respect to the −122 mV prepulse yielded values of h_∞ as shown in Fig. 9 for two

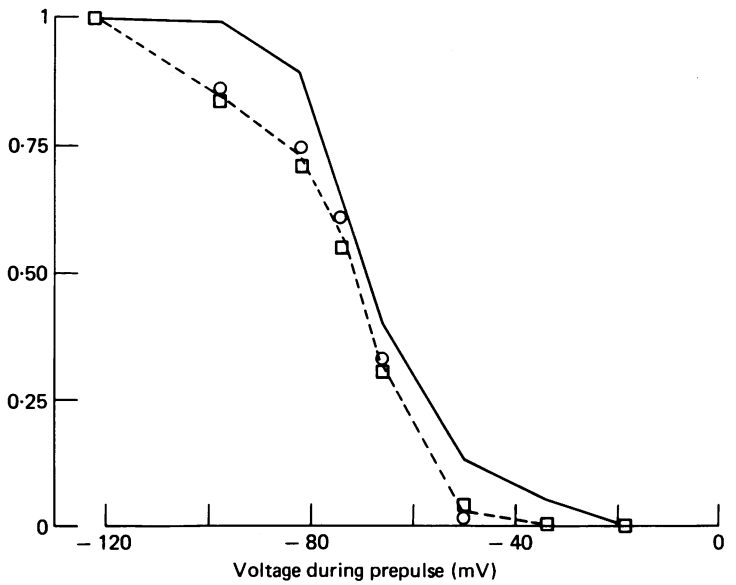

Fig. 9. Voltage dependencies of inactivation and immobilization. Values of h_∞ from two fibres (23/77, □, and 24/77, ○) and mean (dashed line), determined from Na peak currents after 45 msec prepulses; normalized to −122 mV. The continuous line, representing immobilization in the same fibres, was calculated from the mean charges in Fig. 5*B* as described in text.

experiments (open symbols, mean as dashed line). Gating charges measured in the same nodes have already been presented in Fig. 5*B*. Charge immobilization saturated at a finite level as depolarization increased, whereas Na inactivation proceeded to an undetectable level.

A curve more similar to h_∞ was obtained if only the *variation* of the mobile charge was considered. The solid line in Fig. 9 was calculated from the mean charges in Fig. 5*B* by subtracting the minimum value, measured at −18 mV, and normalizing with respect to −122 mV. This procedure would remove any background of charge rearrangements not affected by conditioning. If charge immobilization were due to a single, major transition between states of Na channels, the resulting curve would reflect the fraction of unaffected channels. In this case, the result may directly be compared to h_∞ which is thought to represent the fraction of Na channels that have not undergone the all-or-none step of inactivation (Conti *et al.* 1976; Sigworth, 1977).

The comparison between the curves in Fig. 9 shows that both quantities depend in a very similar, but not identical, way on voltage. With the normalization used, the deviations are in the direction expected if more channels reach the inactivated state(s)

than reach the state(s) of reduced charge movement. The difference is largest at moderately hyperpolarizing voltages, as the inactivation curve is quite asymmetrical with respect to its midpoint. Similar differences were seen in two other experiments.

Kinetics of Na inactivation and of charge immobilization

The kinetic relations between the immobilization of gating charge and the inactivation of Na current were examined with two methods. In the first, the reduction

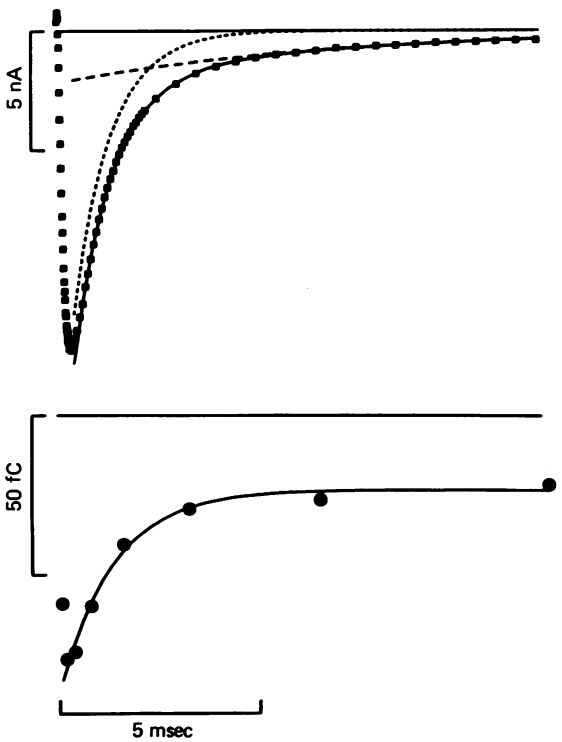

Fig. 10. Decay of Na current and reduction of fast charge movement during depolarization. Top: Na (plus gating) current during test pulse to −6 mV (squares); its decay was fitted by the sum of two exponential (continuous line); exponentials (dashed lines) had time constants of 0·94 and 6·7 msec and amplitudes (extrapolated to beginning of pulse) of −18·1 and −2·2 nA. Bottom: charge carried by fast gating current upon repolarization to −98 mV from test pulses of various durations, plotted *vs.* duration of pulse (records were corrected for slow current by subtracting mean current between 0·3 and 0·6 msec, and integrated from 0 to 0·3 msec). The solid line represents an exponential (time constant 1·33 msec) plus constant. Fibre 6/78; 13 °C. Test pulses applied from −98 mV, control pulses from −122 mV (K = 2).

of fast charge able to return after pulses of various durations was compared to the decay of Na current during a long depolarizing pulse (compare Fig. 8). This method was applicable at voltages less negative than −45 mV. The second method measured, after conditioning pulses of various lengths, how much Na current or mobile gating charge was available during a test pulse to +10 mV. It was used for exploring voltages more negative than −45 mV, and, in particular, for studying both development and reversal of inactivation at the same voltage.

Fig. 10 (upper part) shows the time course of Na current during the first 12 msec of a pulse to −6 mV (squares). After the rapid activation, the current decayed in a way not described by a single exponential function. A better fit was obtained with the sum of two exponentials (continuous line), yielding time constants of 0·94 ± 0·01 and 6·7 ± 0·2 msec for the fast and the slow phase (dashed lines). For comparison, the

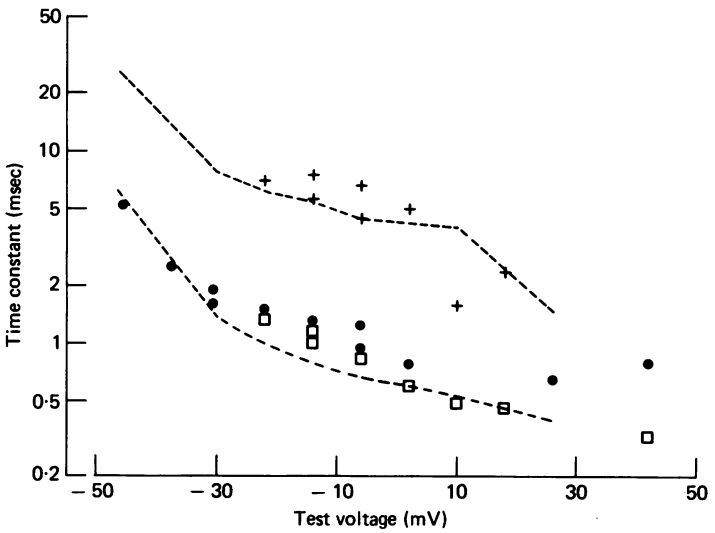

Fig. 11. Time constants of Na inactivation and of charge immobilization versus voltage. Time constants of fast (□) and slow phase (+) of Na inactivation, and of charge immobilization (●) from the same fibres; nine experiments (15/77: −46 and 2 mV; 16/77: −38 mV; 17/77: −30 mV; 18/77: −30 mV; 19/77: −22 and +26 mV; 20/77: 42 mV; 21/77: −14 and −6 mV; 22/77: 42 mV; 6/78: −6 mV). Dashed lines give time constants of fast and slow inactivation (mean of two other experiments, 39/77: and 40/77, where only Na current was studied). On the average, the relative standard deviations of the time constants were: 0·04 (□), 0·13 (+), and 0·15 (●). All experiments at 13 °C. Note logarithmic ordinate.

lower part of Fig. 10 represents measurements of the fast, reverse flow of gating charge, plotted *versus* the length of the pulse (symbols). This decay was described by a single exponential with a time constant of 1·33 ± 0·2 msec (line), corresponding approximately to the smaller time constant of Na inactivation.

Measurements as in Fig. 10 were repeated with different test voltages between −46 and +42 mV; on each node one or two voltages were explored. Time constants from these experiments have been plotted in Fig. 11 on a semilogarithmic scale *vs.* voltage. Open symbols refer to the fast, and crosses to the slow, phase of inactivation; filled symbols represent time constants of charge immobilization. The experiments with small depolarizations were first done with pulses too short for a reliable measurement of the slow phase of inactivation. Therefore, additional measurements of inactivation were made on two other nodes; their mean time constants are given by the dashed lines. The position of the filled symbols suggests a relation between the immobilization of gating charge and the fast phase of Na inactivation. Closer inspection, however, reveals that time constants of immobilization are slightly, but systematically, larger than those of inactivation.

Varying the depolarization changed the relative size of the fast and slow components of Na inactivation. Extrapolated to the beginning of the pulses, the amplitude of the slow component was about 0·2, 0·11, or 0·07 of that of the fast component when the

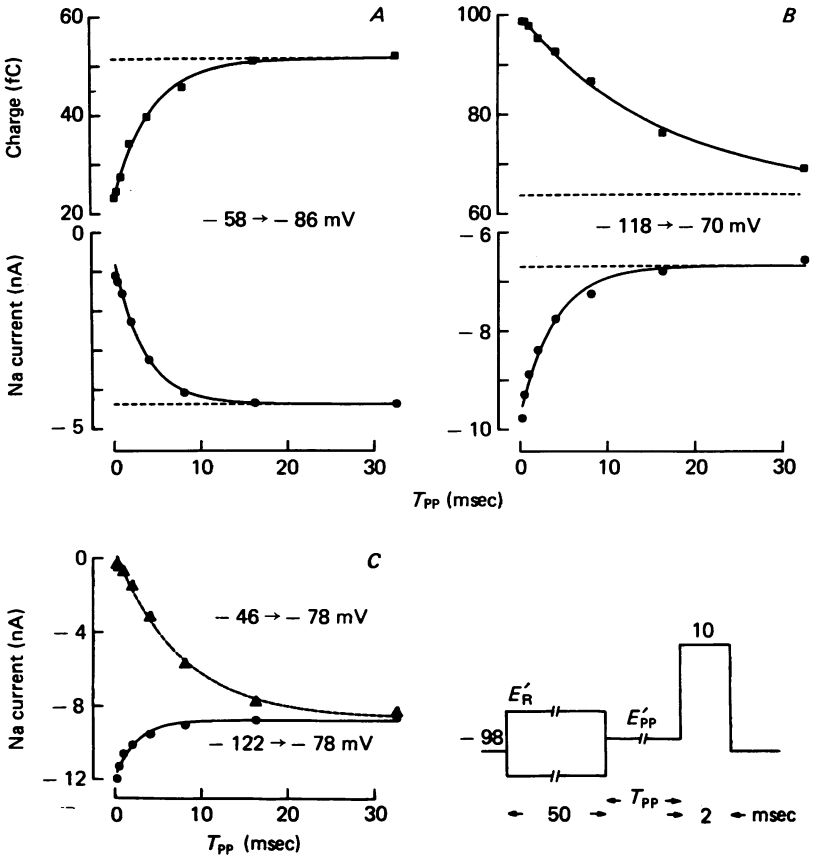

Fig. 12. Development and removal of inactivation and immobilization. Experiments with conditioning prepulses (inset); labels indicate $E'_R \rightarrow E'_{PP}$. *A*, recovery at −86 mV: fast charge movement (top) and Na peak current (bottom) *vs.* recovery interval (T_{PP}). *B*, corresponding time courses of development at −70 *mV*. *C*, time courses of reduction and of recovery at the same actual voltage, −78 *mV* (Na current only). Continuous lines represent exponential plus constant (dashed lines); time constants as in Table 1. Fibres 30/77 (*A*), 32/77 (*B*), and 34/77 (*C*); 13 °C. Control pulses (not shown) according to eqn. (1) with $E''_R = -122$ mV, $K = 2$.

membrane was depolarized to −30, −10, or +10 mV. On the other hand, the ratio between the fast and slow time constants (Fig. 11) was almost constant. It seems, thus, unlikely that the slow component is due to a fixed fraction of Na channels that inactivate more slowly than the bulk of the channels. A consistent explanation would be that the inactivation of a Na channel is a multi-step process. This view is supported by the experiments described in the next section.

The comparison of immobilization with inactivation was extended to more negative potentials by the second kinetic method, using 3-pulse programmes like that in Fig. 12.

The first pulse was chosen either to produce full Na inactivation or to remove it completely. Then, the voltage to be studied was applied for a variable time, during which immobilization or inactivation could develop or reverse. Finally, the available charge or Na current was measured with a test pulse to + 10 mV.

TABLE 1. Time constants from experiments with conditioning pulses

Experiments	E'_R (mV)	E'_{PP} (mV)	τ_h (msec)	τ_b (msec)
A (recovery)				
31/77	−58	−110	1·3 ± 0·05	1·7 ± 0·2
30/77		−102	1·74 ± 0·05	2·5 ± 0·2
29/77		−94	2·55 ± 0·08	3·6 ± 0·2
30/77		−86	3·36 ± 0·08	4·3 ± 0·4
31/77			3·94 ± 0·1	6·8 ± 0·9
29/77		−78	5·8 ± 0·3	7·1 ± 0·5
34/77	−46	−78	7·5 ± 0·8	7·2 ± 0·6
35/77			6 ± 0·5	9·5 ± 1·4
7/78			6·9 ± 0·5	
9/78		−74	6·6 ± 0·5	6·5 ± 1
8/78		−70	12·9 ± 2·2	
B (development)				
34/77	−122	−78	2·5 ± 0·5	*
35/77			1·8 ± 0·3	*
7/78			4·1 ± 0·7	
9/78	−118	−74	3·6 ± 0·6	20 ± 8
32/77		−70	3·9 ± 0·7	16·7 ± 1·9
8/78			6·2 ± 0·7	
33/77	−122	−62	6 ± 0·9	16 ± 3·3
32/77		−54	8·7 ± 0·4	9·4 ± 0·7
33/77		−46	7·7 ± 0·3	7·6 ± 0·4

* During the 30 msec period of conditioning, the charge decayed almost linearly.
Standard deviations of the time constants were obtained from the least-squares fit with the method of Gauss.

Fig. 12*A* shows time courses of recovery at −86 mV, following a depolarization to −58 mV. The available gating charges (top) and Na peak currents (bottom) have been plotted as symbols *vs.* the recovery interval at −86 mV. The fit with a single exponential function (curves) revealed similar time constants, 4·3 ± 0·4 msec for the charge and 3·36 ± 0·08 msec for Na current. A similarity of recovery time constants was found also at other voltages between −110 and −70 mV (Table 1*A*). In all experiments, the early values of Na peak current deviated from the exponential time course by a delay, which was not reflected in the recovery of gating charge. This delay became larger as the voltage during recovery was made more positive (compare upper trace of Fig. 12*C*).

By contrast to the similarity of recovery time courses, the time courses for development of immobilization and inactivation near the resting potential were markedly different. Fig. 12*B* shows an experiment at −70 mV, where the fit with single exponentials (curves) revealed time constants of 3·9 ± 0·7 msec (Na current) and 16·7 ± 1·9 msec (charge). In other experiments (Table 1*B*), the difference was even stronger

at a small hyperpolarization and it became smaller as the voltage became more positive. Further, both time courses deviated in different ways from the exponential function. Immobilization developed with a small delay, whereas inactivation showed indication of a fast and a slow phase. Indeed further evidence for complexities of inactivation in this voltage range is the finding that development and removal of Na inactivation have quite different time courses when measured at the same voltage. Fig. 12*C* shows an experiment at −78 mV where the fit with single exponentials (curves) yields different time constants, 7·5 ± 0·8 msec (recovery) and 2·5 ± 0·5 msec (development) and there are the deviations from the exponential time course mentioned before, a delayed removal and a biphasic development of inactivation. The difference was observed at voltages between −78 and −70 mV (Table 1).

Together, the relaxation experiments suggest that inactivation of nodal Na channels is a multi-step process. The immobilization of gating charge reflects Na inactivation in some cases, and not in others. These results will be discussed in detail later in terms of a model with several states of inactivation some of which are also 'immobilized'.

DISCUSSION

The results confirm previous observations that depolarization reduces the rapid part of the gating current in the node of Ranvier (Neumcke *et al.* 1976; Nonner *et al.* 1978), and reveal further details of the phenomenon. Thus, the reduction of transferred charge is incomplete even with depolarizing prepulses of 45 msec duration, leaving about one third of the maximum charge movement between voltages of −122 and +10 mV (Fig. 5). Movements of the non-immobilized charge depend less strongly on voltages than the normal ones, both in kinetics (Figs. 5*C*, 6) and in steady-state (Figs. 6, 7). These results are in qualitative agreement with observations on squid giant axons (Armstrong & Bezanilla, 1974, 1976; Bezanilla & Armstrong, 1974, 1975; Meves & Vogel, 1977). Further a paradoxical effect of the preceding depolarization has been detected with test voltages near the resting potential. There, the amplitude of the gating current, as well as the size of the charge, do not decrease, but increase, as if the conditioning depolarization recruited a kind of charge movement not present in the previously hyperpolarized membrane (Figs. 6, 7). Such a charge movement may reflect a modified kind of rearrangement of the same structures that produce the normal gating current. This point is considered again later.

The immobilization of nodal gating charge corresponds in several respects to the inactivation of Na current, showing parallels in the steady-state dependence on voltage (Fig. 9) and the time courses of development during a depolarization (Figs. 10, 11) and of recovery after a depolarization (Fig. 12, Table 1*A*). Again, these results compare to those on squid axons. Armstrong & Bezanilla (1977) found a close correlation in all three properties. Meves & Vogel (1977) report qualitatively similar results, but, in their experiments, inactivation developed about four times faster than immobilization and only one half of the charge could be immobilized. Thus, in both kinds of nerve, gating current reflects properties of both Na activation and inactivation, indicating that a large fraction of the measured gating current is, in fact, due to the gating process of Na channels. From the criterion of immobilization, a minimum of two thirds of the fast charge movement in a node may be assigned to Na channel

gating. The fraction may be even larger, since at least part of the non-immobilized charge moves only after a depolarization (Figs. 6, 7). This view is supported by recent experiments on squid axons: internal *N*-methylstrychnine (Cahalan & Almers, 1979) or pancuronium (Armstrong & Yeh, 1978), which block ionic current in open Na channels, suppress also the immobilization-resistant movement of charge. From this criterion, Cahalan & Almers estimated a lower limit of 90% for the fraction of true gating charge.

The immobilization of gating charge has been interpreted in terms of coupled activation and inactivation processes (Armstrong & Bezanilla, 1977). If inactivation were otherwise a first-order process, one would expect non-exponential relaxations only when activation is changing, for example, a short delay in the onset of inactivation upon a step depolarization (Bezanilla & Armstrong, 1977). In the node of Ranvier, however, deviations from the first-order kinetics are observed at later times. Thus, Na current decays in two phases during a maintained depolarization (Figs. 10, 11), it recovers after a delay (Fig. 12*A*, *C*), and at the same actual voltage, it inactivates more rapidly than it recovers (Fig. 12*C*, Table 1). These results are in line with a study by Chiu (1977), performed at low temperature (4·5 °C), and suggest that inactivation *per se* is a high-order process (Hille, 1976). If this is true, which part of the process is reflected by the immobilization of gating charge?

The simplest high-order scheme that may describe the results is the inactivation scheme of Chiu (1977), which provides one more closed state of inactivation than the original scheme of Hodgkin & Huxley (1952):

$$h_1 \underset{\text{(open)}}{\overset{\text{(fast)}}{\rightleftharpoons}} h_2 \underset{\text{(closed)}}{\overset{\text{(slow)}}{\rightleftharpoons}} h_3 \quad \text{(closed)}$$

Both transitions depend on voltage. In state h_1, the channel may pass Na ions provided it becomes activated; in states h_2 and h_3, the ionic pathway is closed, regardless of activation. We now examine whether immobilization of gating charge could be attributed to one of the transitions in this model.

Consider the relaxations observed with a step depolarization (Fig. 10). Na current and gating charge decline with similar time courses. Close inspection reveals that the time course of immobilization can be described by a single exponential, whereas two exponentials are required for describing the time course of Na inactivation. On the other hand, time constants of immobilization are found to be slightly larger than those of the fast inactivation (Fig. 11). This would be expected if a small slow component were also present in immobilization and would affect the fits with a single exponential. In any case, the properly rescaled time courses of Na inactivation would superimpose the decays of gating charge quite well. Thus, charge immobilization and Na inactivation seem to reflect the same event, and, in Chiu's scheme, the open-closed transition ($h_1 \rightarrow h_2$) must be postulated to restrict the movement of gating charge as well as to inactivate the channel.

This assignment, however, does not hold under other experimental conditions. Near the resting potential, Na inactivation *develops* significantly faster than charge immobilization (Fig. 12*B*, Table 1), and it proceeds in two phases, while immobilization starts with a delay. Further, although *recovery* time courses are similar at later times,

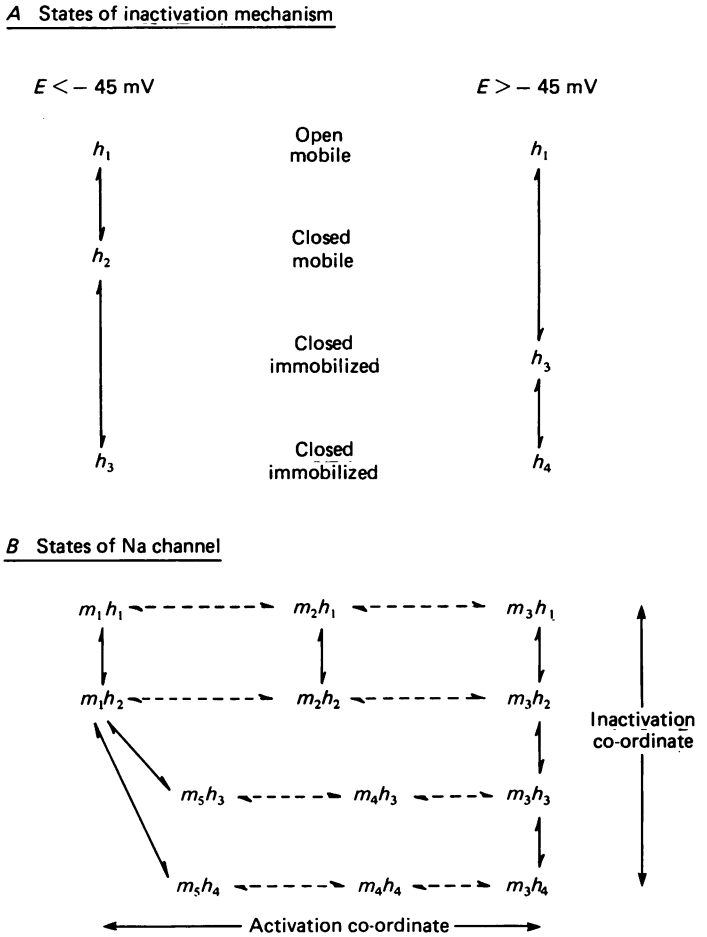

Fig. 13. *A*, states of inactivation mechanism. Left graph: experiments with conditioning pulses; right graph: experiments with maintained depolarizations. *B*, states of Na channel. Dashed arrows: fast transitions of activation; filled arrows: slower transitions of inactivation (vertical) or of both activation and inactivation (diagonal). Only state $m_3 h_1$ is conducting. *C*, free energies, $\triangle G$, and valencies, *Z*, of equilibrium and transition (▲) states. The free energies (ordinate) are given for the resting potential, − 70 mV. Equilibrium levels of inactivation: ○, open; ●, closed, mobile; ■, closed, immobilized. Dashed and continuous lines as in *B*. Note interrupted energy scale.

they reveal a delay of inactivation, but not of immobilization (Fig. 12*A*, *C*). In the steady state, inactivation is stronger than immobilization, particularly at hyperpolarizing voltages (Fig. 9). These observations are compatible with Chiu's scheme only if charge immobilization is ascribed to the second transition, $h_2 \rightarrow h_3$, in contradiction to the conclusion reached in the previous paragraph.

In order to avoid the conflict, one could consider to extend the scheme by a direct transition $h_1 \rightleftharpoons h_3$. This transition could account for parallel time courses as in Fig. 10 if it were preferred upon depolarization. To the same extent, however, the system would approach first-order kinetics, and no longer predict a slow phase of Na inactivation.

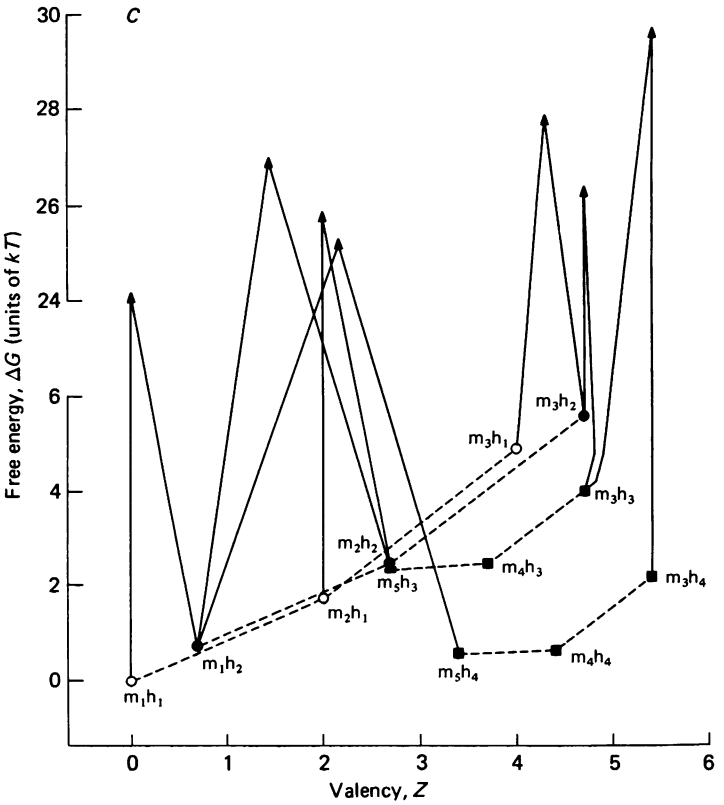

Fig. 13*C*. For legend see opposite.

Apparently, immobilization and inactivation reflect a process of higher-than-second order that, under different experimental conditions, becomes similar to one or the other of the second-order processes discussed. Fig. 13*A* represents the second-order schemes after a relabelling and rearranging of states. The right side refers to experiments with step depolarizations (Fig. 10): a first, fast transition blocks Na current and immobilizes gating charge; it is followed by a slow transition not directly reflected in Na or gating current. The left side refers to experiments with conditioning pulses (Figs. 9, 12): a first, fast transition blocks Na current; a second, slow transition immobilizes gating charge. The schemes are now recognized as particular cases of a third-order scheme with states h_1 through h_4, where either h_3 (left side) or h_2 (right side) are virtually unoccupied states. Thus, a third-order scheme may be able to describe the kinetics of inactivation and of the related immobilizing effect on the gating charge.

Inactivation may block gating charges in various ways. (1) It raises the energy barrier for the displacement of charges. In this case, inactivation would derive no voltage dependence from the coupling to the fast charge movement, and separate charges or dipoles have to exist for controlling inactivation. (2) It excludes gating charges from certain equilibrium states, e.g. if an inactivation subunit occupied positions that could otherwise be occupied by gating particles. Then inactivation could derive its voltage dependence, or part of it, from the coupling to the fast charge

movements. (3) It combines (1) and (2). In this case, rate constants of inactivation would generally depend on the configuration of gating charge and vice versa.

Case (1) appears extreme and rather unlikely. Case (2) would account for a block of charge movement, but would not predict that a new kind of charge movement appears after depolarization (Figs. 6, 7). The general case (3) would be consistent with the last observation and also could explain two other, possibly related observations. The first is the particular voltage dependence of inactivation rates that has been found in nerve and muscle fibres (see, for example, Campbell & Hille, 1976, their Fig. 7, for a comparison between results obtained by describing inactivation as a first-order process, and Chandler & Meves, 1970, for an analysis in terms of a second-order process). These rates vary steeply with small depolarizations, but less steeply, or not at all, with large depolarizations. The steep change may reflect a redistribution of gating charges that is associated with a change in the inactivation rate. The second observation is that, in the node of Ranvier, the kinetics of charge immobilization and inactivation are closely similar positive to -45 mV, but dissimilar at more negative potentials (compare Fig. 13*A*). The transition between these two kinds of behaviour occurs at a voltage where the distribution curve of the charges, and changes in the activation process, are steep.

The fast movement of gating charge is thought to be involved in the activation of Na channels, though a state diagram of this process has not yet been designed (cf. the reviews of Meves, 1978; Almers, 1978; Neumcke *et al.* 1978). States of the gating charge will in the following be tentatively referred to as m_1, m_2, and so on, as if they were equivalent to states of activation.

The above considerations may now be summarized in a state diagram as in Fig. 13*B*. Here, the linear sequence of inactivation states has been split into as many sequences as there are states of activation. For simplicity, activation states have been assumed to form linear sequences as well. In inactivation levels h_1 or h_2 (where charge is not immobilized), activation can undergo unrestricted transitions between m_1 and m_3, thereby stepping through m_2 and other intermediate states (not shown). In the inactivation levels h_3 or h_4, activation may rapidly change between m_3 and some state m_5, but can reach m_1 only by a simultaneous, slow transition of inactivation into level h_2 (diagonal arrows). Further, rate constants of inactivation may be different for the various states of activation and vice versa.

The second part of this paper gives a quantitative analysis and further discussion of such a model.

PART II: A MODEL FOR Na INACTIVATION

This section explores, as an example of models with interacting activation and inactivation processes, the model defined by the state diagram of Fig. 13*B*.

MATHEMATICAL FORMULATION OF THE MODEL

The model is formulated in terms of absolute rate theory. Rate constants are defined as simple exponential functions of voltage.

Each channel state, $m_i h_j$, is assigned a difference in free energy, ΔG_j^i, relative to

state $m_1 h_1$. Free energies are measured in units of kT (24·7 meV at 13 °C) and split into a 'chemical' and an 'electrical' term:

$$\Delta G_j^i = \Delta W_j^i - Z_j^i U, \tag{2}$$

where U is the reduced voltage $U = eE/kT$ (kT/e = 24·7 mV at 13 °C), and Z_j^i is an effective valency describing the effect of the membrane voltage on the configuration changes of the channel: transforming the channel from state $m_1 h_1$ into state $m_i h_j$ decreases its potential energy in the electrical field of the membrane as much as that of a particle with Z_j^i positive elementary charges moved from a location of electrical potential E to another location of potential zero. Thus, Z_j^i describes any molecular mechanism of charge rearrangement.

Transitions between states $m_i h_j$ and $m_1 h_n$ are assumed to happen *via* a 'transition' state with the free-energy difference

$$\Delta G_{jn}^{il} = \Delta W_{jn}^{il} - Z_{jn}^{il} U. \tag{3}$$

Absolute rate theory (Glasstone, Laidler & Eyring, 1941) yields for the rate coefficients of transition from state $m_i h_j$ to state $m_1 h_n$

$$K_{jn}^{il} = C(kT/h) \exp(-[\Delta G_{jn}^{il} - \Delta G_j^i]), \tag{4}$$

where $(kT/h) = 5{\cdot}96 \times 10^{+12}$ sec^{-1} at 13 °C. The 'transmission coefficient' C is assumed to be one.

The scheme of Fig. 13*B* describes fast and slow reactions with rates differing by one or two orders of magnitude. Since only the slow relaxations, namely those related to inactivation, will be compared to experiment, the analysis is simplified by assuming that a thermodynamic equilibrium between rapidly exchanging states (horizontal transitions) is maintained during the slower (vertical or diagonal) transitions. The probability of a channel state $m_i h_j$ is then represented by

$$P_j^i = P_j \times B_j^i, \tag{5}$$

where P_j represents the probability that a channel is in the inactivation level h_j, and

$$B_j^i = \exp[-\Delta G_j^i]/(\sum_l \exp[-\Delta G_j^l]) \tag{6}$$

gives the conditional probability that the channel is in activation state m_i provided that the inactivation level is h_j. (For justification of this approach confer to Colquhoun & Hawkes, 1977.)

The transitions between inactivation levels are described by four linear differential equations

$$\dot{P}_1 = -D_1 P_1 + D_2 P_2, \tag{7}$$
$$\dot{P}_2 = D_1 P_1 - (D_2 + D_3 + D_7) P_2 + D_4 P_3 + D_8 P_4, \tag{8}$$
$$\dot{P}_3 = D_3 P_2 - (D_4 + D_5) P_3 + D_6 P_4, \tag{9}$$
$$\dot{P}_4 = D_7 P_2 + D_5 P_3 - (D_6 + D_8) P_4, \tag{10}$$

where

$$D_1 = B_1^1 K_{12}^{11} + B_1^2 K_{12}^{22} + B_1^3 K_{12}^{33}, \tag{11}$$
$$D_2 = B_2^1 K_{21}^{11} + B_2^2 K_{21}^{22} + B_2^3 K_{21}^{33}, \tag{12}$$
$$D_3 = B_2^1 K_{23}^{15} + B_2^3 K_{23}^{33}, \tag{13}$$
$$D_4 = B_3^5 K_{32}^{51} + B_3^3 K_{32}^{33}, \tag{14}$$

$$D_5 = B_3^3 K_{34}^{33}, \tag{15}$$
$$D_6 = B_4^3 K_{43}^{33}, \tag{16}$$
$$D_7 = B_2^1 K_{24}^{15}, \tag{17}$$
$$D_8 = B_4^5 K_{42}^{51}. \tag{18}$$

As an additional restriction, probabilities must be normalized:

$$P_1 + P_2 + P_3 + P_4 = 1. \tag{19}$$

The solutions are of the form (Colquhoun & Hawkes, 1977)

$$P_l = P_{l,\infty} + \sum_{j=1}^{3} P_{l,j} \exp[-t/\tau_j], \tag{20}$$

where $P_{l,\infty}$ is the steady-state probability of inactivation level h_l, and $P_{l,j}$ represents amplitudes of three exponential terms in τ_j that contribute to the time course of relaxation. From these solutions, the kinetics of three quantities may be derived:

(1) the inactivation variable h, which is identical to P_1:

$$h = h_\infty + h_1 \exp(-t/\tau_1) + h_2 \exp(-t/\tau_2) + h_3 \exp(-t/\tau_3) \tag{21}$$

(2) an immobilization variable b representing the probability that the full charge movement is available in a channel, which is the sum of P_1 and P_2:

$$b = b_\infty + b_1 \exp(-t/\tau_1) + b_2 \exp(-t/\tau_2) + b_3 \exp(-t/\tau_3) \tag{22}$$

(3) the gating charge q displaced with respect to state $m_1 h_1$ (in units of elementary charges per channel):

$$q = q_\infty + q_1 \exp(-t/\tau_1) + q_2 \exp(-t/\tau_2) + q_3 \exp(-t/\tau_3). \tag{23}$$

The last coefficients are calculated from

$$q_\infty = \sum_j P_{j,\infty} \left(\sum_i B_j^i Z_j^i\right) \tag{24}$$

$$q_k = \sum_j P_{j,k} \left(\sum_i B_j^i Z_j^i\right) \tag{25}$$

Step changes of voltage produce continuous relaxations in h and b, but a step transition and a subsequent continuous relaxation in q (the step transition occurs because changes between activation states have been treated as if they were infinitely fast).

This completes the quantitative formulation of the model. For given free energies ΔW and valencies Z, the quantities h, b, and q may be calculated with standard numerical methods. An algorithm suitable for minicomputers will be described elsewhere (F. Conti, B. Neumcke, W. Nonner & R. Stämpfli, in preparation). In the following, the quantities h, b, and q are referred to in the form of eqns. (21)–(23). The largest time constant is labelled τ_1, the smallest τ_3.

RECONSTRUCTION OF THE EXPERIMENTAL CURVES

This section describes the procedure of finding parameters and compares experimental and theoretical results.

The model was represented in a computer program that received values of the parameters and calculated steady-state variables, amplitudes and time constants of relaxations, or time courses of relaxations. The results were plotted versus voltage or time on a display screen, together with the experimental points for comparison. Simple or compound rate coefficients, K or D, were listed for a few voltages. Further, the program displayed an extended free-energy diagram of the model as in Fig. 13*C*. Each equilibrium or transition state was assigned an ordinate corresponding to its free energy, ΔG, and an abscissa corresponding to its valency, Z, relative to state $m_1 h_1$, which is at the origin. A very useful feature of such a free-energy diagram is that one can readily visualize the effect of voltage changes by inspection. Fig. 13*C*

TABLE 2. Parameters of the inactivation model

A (equilibrium states)			
ΔW_1^2	−3·94	Z_1^2	2
ΔW_1^3	−6·49	Z_1^3	4
ΔW_2^1	−1·30	Z_2^1	0·7
ΔW_2^2	−5·24	Z_2^2	2·7
ΔW_2^3	−7·79	Z_2^3	4·7
ΔW_3^3	−9·35	Z_3^3	4·7
ΔW_3^4	−8·02	Z_3^4	3·7
ΔW_3^5	−5·30	Z_3^5	2·7
ΔW_4^3	−13·15	Z_4^3	5·4
ΔW_4^4	−11·82	Z_4^4	4·4
ΔW_4^5	−9·10	Z_4^5	3·4
B (transition states)			
ΔW_{12}^{11}	24	Z_{12}^{11}	0
ΔW_{12}^{22}	20	Z_{12}^{22}	2
ΔW_{12}^{33}	15·5	Z_{12}^{33}	4·3
ΔW_{23}^{15}	22·7	Z_{23}^{15}	1·45
ΔW_{23}^{33}	13	Z_{23}^{33}	4·7
ΔW_{24}^{15}	19	Z_{24}^{15}	2·15
ΔW_{34}^{33}	14·2	Z_{34}^{33}	5·4

The changes of Gibbs free energy, ΔW, are given with respect to state $m_1 h_1$ and are in units of kT (24·7 meV at 13 °C).

was drawn for the resting potential. Depolarization would reduce the free energies (ordinate) in proportion to valency (abscissa), a transformation equivalent to distorting the rectangular co-ordinates to form a parallelogram by lowering the right hand side of the diagram while keeping the left-hand side fixed. Such graphs were used for orientation and illustrate the concept of the fitting procedure used.

The model provided thirty-six free parameters: the coordinates of eleven equilibrium and of seven transition states (Fig. 13*C*). Microscopic reversibility was ensured for any choice of these parameters. Steady-state or kinetic properties of the model were separately adjusted by varying the coordinates of equilibrium or of transition states. Sixteen parameters were eliminated by assigning certain states fixed positions relative to others. The remaining parameters were found by trial and error. Agreement with the experiment was judged by eye, and new parameters were entered to the computer by hand. The following section gives details of the procedure. The final parameters are summarized in Table 2.

Equilibrium states

The diagram of Fig. 13*C* shows four pathways (dashed lines) along which equilibria between rapidly exchanging states of activation (or charge arrangement) are maintained. Such states were given fixed relative positions, e.g.

$$\Delta W_2^2 = \Delta W_2^1 + \Delta W_m - kT\ln 2, \quad Z_2^2 = Z_2^1 + Z_m,$$
$$\Delta W_2^3 = \Delta W_2^1 + 2\Delta W_m, \quad Z_2^3 = Z_2^1 + 2Z_m.$$

This is equivalent to the simplifying assumption that activation is due to the displacement, from a resting to a permissive position, of two equal and independent gating subunits, the displacement of a subunit being governed by ΔW_m and Z_m. With the values of ΔW_m and Z_m chosen for the inactivation levels h_1 and h_2, $-3{\cdot}24\ kT$ and 2, steady-state activation was one half near -29 mV and its steepest change was e-fold per 6·2 mV. Immobilization of the activating subunits (as occurring at inactivation levels h_3 and h_4) was represented by lowering the values of ΔW_m and Z_m to $-2{\cdot}03\ kT$ and 1. Then, the fast charge movement was reduced to one half, and the steepness of the charge distribution curve was reduced to one half with the midpoint shifted towards -50 mV.

With these relations, absolute co-ordinates had to be found only for three of the equilibrium states, e.g. m_1h_2, m_3h_3, m_3h_4. State m_3h_3 was assigned the same valency as state m_3h_2 because there was no reason to give step m_3h_2–m_3h_3 a voltage dependence. Since some voltage sensitivity of the step m_3h_3–m_3h_4 was required to account for the voltage dependence of the longer time constant of inactivation (Fig. 11), state m_3h_4 was attributed a larger valency than state m_3h_3. The co-ordinates of state m_1h_2 and the ordinate of state m_3h_4 were adjusted to predict the observed steady-state curves of Fig. 9, while state m_3h_3 was assigned a preliminary ordinate, intermediate to states m_3h_1 and m_3h_4. The final ordinate of state m_3h_3 was found from relaxations, as described below. In Fig. 14*A*, the steady-state measurements have been replotted, together with the theoretical curves. The difference between steady-state inactivation and immobilization is mainly interpreted as the occupancy of state m_1h_2, as may be recognized from Fig. 13*C*.

Transition states

Valencies of transition states were restricted to range between the valencies of the associated equilibrium states. Rate constants of the transitions m_1h_1–m_1h_2 and m_2h_1–m_2h_2 were assumed to be identical, as if activation and inactivation were mutually independent in these states.

Inactivation was postulated to vary, dependent on voltage, along one of two main pathways (Fig. 13*A*). Upon a depolarization (activating more than half of the channels), the way m_3h_1–m_3h_2–m_3h_3–m_3h_4 had to be preferred; m_3h_2–m_3h_3 had to become the fastest, m_3h_3–m_3h_4 the slowest transition. Therefore, transition states were chosen such that the largest time constant of relaxation, τ_1, was mainly sensitive to ΔG_{34}^{33} and reproduced the larger time constant of Na inactivation (Fig. 11), whereas the intermediate time constant, τ_2, was mainly determined by ΔG_{12}^{33} and reflected the smaller time constant of Na inactivation. The ratio between the amplitudes of both relaxations was adjusted by varying ΔW_3^3.

At rest or at more negative voltages, the pathway $m_1 h_1$–$m_1 h_2$–$(m_5 h_3) m_5 h_4$ had to prevail. ΔG_{23}^{15} and ΔG_{24}^{15} were chosen to yield similar time constants τ_1 and τ_2; these were adjusted to the observed recovery time constants of inactivation (Table 1*A*).

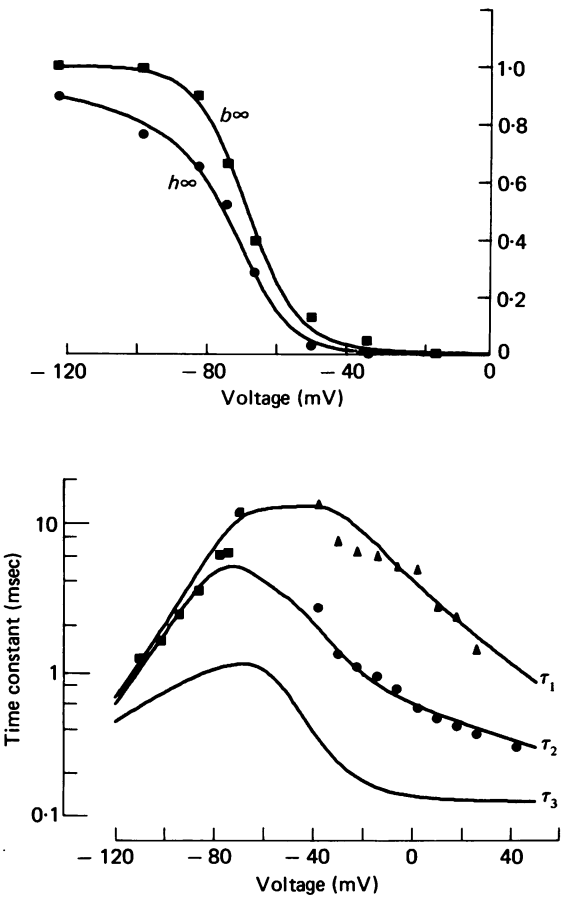

Fig. 14. *A*, steady-state inactivation (●) and immobilization (■) from experiment (Fig. 9) and theory (lines) *vs.* voltage. The experimental points of inactivation were rescaled by the factor 0·896 corresponding to theoretical h_∞ at $E = -122$ mV. *B*, time constants from experiment (symbols) and theory (lines) *vs.* voltage. Symbols: ●, fast and, ▲, slow time constants measured from inactivation (mean values from Fig. 11); ■, mean recovery time constants of inactivation from Table 1*A*.

ΔW_{12}^{11} was chosen to maintain sufficiently large time constants τ_2 at intermediate voltages where both pathways of inactivation were used. Z_{12}^{11} was assumed to be zero; thus the transition $m_1 h_1$–$m_1 h_2$ did not become rate limiting within the explored range of hyperpolarization. The three theoretical time constants are represented in Fig. 14*B*, together with comparable time constants from the experiments. These curves reveal a complex dependence on voltage, though all individual rate constants are simple exponentials in voltage.

Theoretical time courses of inactivation and immobilization are shown in Fig. 15. The curves correspond to the experimental time courses of Fig. 12(*A–C*) and Fig.

10 (*D*). The agreement between theory and experiment appears good if one considers that no attempt was made to reconstruct the individual experiments: all curves are calculated with the parameters of Table 2. In particular, the model predicts the deviations from the exponential time course discussed in Part I. In Fig. 15*D*, immobilization reveals a larger slow phase than inactivation. It would become more

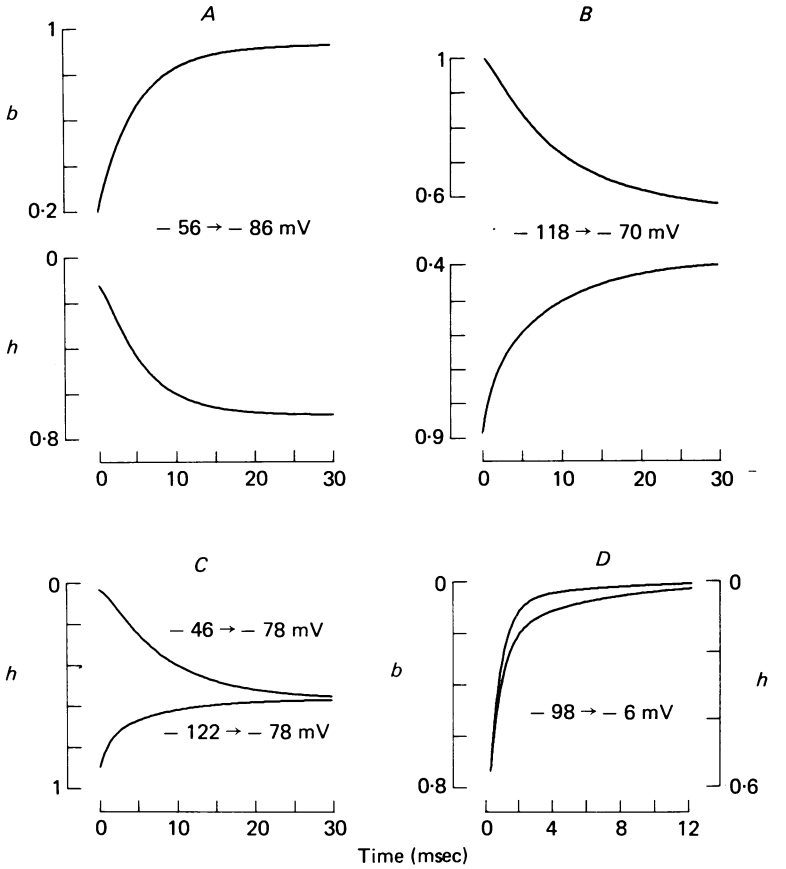

Fig. 15. Theoretical time courses of inactivation and immobilization. *A–C* correspond to experimental time courses of Fig. 12, *D* to the ones of Fig. 10. Inactivation (and immobilization in *D*) plotted at reversed scales facilitating comparison to experiment. All curves calculated from parameters in Table 2.

similar to inactivation if the occupancy of state $m_3 h_2$ were reduced by raising its free energy. This would imply that the distributions of gating charges are different at inactivation levels h_1 and h_2. This point could be examined by studying gating currents after short depolarizing prepulses.

Fig. 16 shows a theoretical simulation of the charge movements in Fig. 8. The model predicts some slow movement of charge during the pulse as well as a growing slow component in the return of charge after the pulse. Apparently, these components would be well contained in the observed slow gating current. In Fig. 16, more than one half of the fast charge movement *seems* to be blocked by long pulses although the

model is laid out such that only half of the mobile charge *can* be blocked. The difference is due to the different distribution curves assigned to normal charges (inactivation levels h_1, h_2) or partially immobilized charges (h_3, h_4), and is the result of two effects. (1) As channels reach inactivation levels h_3 or h_4 *during* the depolarization, some of

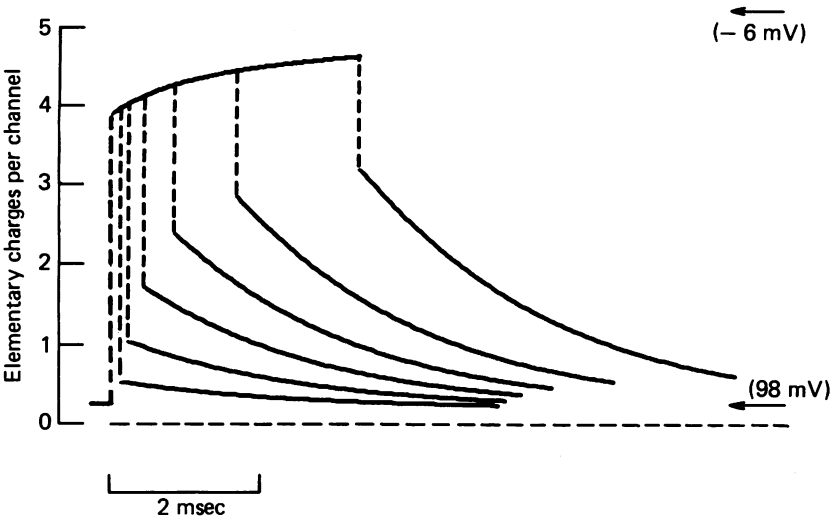

Fig. 16. Theoretical movements of charge. Simulation of the experiment in Fig. 8. Curves represent time course of variable q of theory during and after the depolarizing pulse (rather than net movement of charge from pulse and control pulse). Arrows mark steady-state displacements of charge at -98 and -6 mV. The ordinate gives elementary charges/channel. The fast movements of charge (dashed lines) appear as instantaneous, according to simplified treatment of theory.

their gating charges return already from m_3 to m_4 or m_5 (compensating part of the slow gating current associated with transitions between inactivation levels). (2) *Repolarization* to -98 mV does not return all of the partly immobilized charges from m_3 to m_5; the remainder returns slowly as state $m_5 h_4$ ($m_5 h_3$) is depleted by recovery from immobilization. Such measurements are, thus, able to give ambiguous results on the degree of true immobilization.

DISCUSSION OF THE MODEL

A model of Na inactivation has been analysed in which the inactivation process *per se* is of third order and is thermodynamically coupled to the rapid movement of gating charge. In particular, the numerical calculations have shown that inactivation *can* derive most of its voltage dependence from a fast process that has steady-state characteristics similar to those of activation. This invalidates an argument by Meves (1978) and is in agreement with the idea of Armstrong & Bezanilla (1977). On the other hand, some voltage sensitivity had to be given to inactivation itself in order to predict the small voltage dependence of time constants at large depolarizations. This property, however, could be species dependent.

All of the residual charge movement, resistant to immobilization, was attributed to Na channels in order to make the model consistent with other, not directly related,

observations: removing the states $m_5 h_4$ ($m_5 h_3$) and $m_4 h_4$ ($m_4 h_3$) and introducing a direct path, $m_3 h_4$ ($m_3 h_3$) $\rightarrow m_1 h_2$, would give by far too much voltage dependence, and eliminating that direct path would give too little voltage dependence, to the larger time constant of inactivation at the resting potential and more negative potentials. In the model analysed, *all* of the immobilization-resistent charge movement had to be attributed to the fast transitions between m_5, m_4, and m_3. Other models, with the diagonal transitions (Fig. 13) shifted in *parallel* to the right, would give a higher degree of immobilization, but a less steep change of kinetic behaviour around -45 mV. The other extreme model in which the fast gating charge of Na channels can be totally immobilized (with the diagonal transitions from $m_3 h_3$ and $m_3 h_4$) would be inconsistent with the measurements. In summary, an incomplete immobilization appears to be an essential property of this kind of model, but some part of the observed immobilization-resistant charge might still be attributable to processes not related to gating in Na channels.

Besides immobilization, a further interaction between gating charge and inactivation had to be postulated: the rate constants of the transition $h_1 \rightleftarrows h_2$ had to be larger at m_3 than at m_1 (about 7·5 fold at $E = 0$). Thus, the model became functionally similar to a sequential activation $\rightarrow$ inactivation scheme when the membrane was depolarized. This implies that a relatively large fraction of Na channels conduct before they become inactivated. On the other hand, the Na channels of this model do not become conducting again when they recover: recovery follows mainly the path $m_3 h_4 \rightarrow m_5 h_4 \rightarrow m_1 h_2 \rightarrow m_1 h_1$. This shows how Na channels could be used efficiently and still recover quickly.

I am indebted to Drs Bertil Hille and Wolfhard Almers for discussions and for suggestions concerning the manuscript. Financial support was provided by the Deutsche Forschungsgemeinschaft, Sonderforschungsbereich 38 'Membranforschung', and the National Institute of Health grant no. NS08174 to Dr Hille.

REFERENCES

ALMERS, W. (1978). Gating currents and charge movements in excitable membranes. *Rev. Physiol. Biochem. Pharmacol.* **82**, 96–190.

ARMSTRONG, C. M. & BEZANILLA, F. (1974). Charge movement associated with the opening and closing of the activation gates of the Na channels. *J. gen. Physiol.* **63**, 533–552.

ARMSTRONG, C. M. & BEZANILLA, F. (1976). A slow gating current component during recovery from inactivation. *Biophys. J.* **16**, 27*a*.

ARMSTRONG, C. M. & BEZANILLA, F. (1977). Inactivation of the sodium channel. II. Gating current experiments. *J. gen. Physiol.* **70**, 567–590.

ARMSTRONG, C. M. & YEH, J. F. (1978). Selective block of 'off' gating current. *Bipohys. J.* **21**, 41*a*.

BEZANILLA, F. & ARMSTRONG, C. M. (1974). Gating currents of the sodium channels: three ways to block them. *Science, N.Y.* **183**, 753–754.

BEZANILLA, F. & ARMSTRONG, C. M. (1975). Inactivation of gating charge movement. *Biophys. J.* **15**, 163*a*.

BEZANILLA, F. & ARMSTRONG, C. M. (1977). Inactivation of the sodium channel. I. Sodium current experiments. *J. gen. Physiol.* **70**, 549–566.

CAHALAN, M. D. & ALMERS, W. (1979). Block of sodium conductance and gating current in squid giant axons poisoned with quaternary strychnine. *Biophys. J.* **27**, 57–74.

CAMPBELL, D. T. & HILLE, B. (1976). Kinetic and pharmacological properties of the sodium channels of frog skeletal muscle. *J. gen. Physiol.* **67**, 309–323.

CHANDLER, W. K. & MEVES, H. (1970). Rate constants associated with sodium conductance in axons perfused with sodium fluoride. *J. Physiol.* **211**, 679–705.

CHIU, S. Y. (1977). Inactivation of sodium channels: second order kinetics in myelinated nerve. *J. Physiol.* **273**, 573–596.

COLQUHOUN, D. & HAWKES, A. G. (1977). Relaxation and fluctuations of membrane currents that flow through drug-operated channels. *Proc. R. Soc.* B **199**, 231–262.

CONTI, F., HILLE, B., NEUMCKE, B., NONNER, W. & STÄMPFLI, R. (1976). Measurement of the conductance of the sodium channels from current fluctuations at the node of Ranvier. *J. Physiol.* **262**, 699–727.

GLASSTONE, S., LAIDLER, K. J. & EYRING, H. (1941). *The Theory of Rate Processes.* New York: McGraw-Hill Book Company.

HILLE, B. (1976). Gating in sodium channels of nerve. *A. Rev. Physiol.* **38**, 139–152.

HODGKIN, A. L. & HUXLEY, A. F. (1952). A quantitative description of membrane current and its application to conduction and excitation in nerve. *J. Physiol.* **117**, 500–544.

MEVES, H. (1978). Inactivation of the sodium permeability in squid giant nerve fibres. *Prog. Biophys. molec. Biol.* **33**, 207–230.

MEVES, H. & VOGEL, W. (1977). Inactivation of the asymmetrical displacement current in giant axons of Loligo Forbesi. *J. Physiol.* **267**, 377–393.

NEUMCKE, B., NONNER, W. & STÄMPFLI, R. (1976). Asymmetrical displacement current and its relation with the activation of sodium current in the membrane of frog myelinated nerve. *Pflügers Arch.* **363**, 193–203.

NEUMCKE, B., NONNER, W. & STÄMPFLI, R. (1978). Gating currents in excitable membranes. *MTP International Review of Science* (Biochemistry Series), vol. 2, series 2. London: Butterworths.

NONNER, W. (1969). A new voltage clamp method for Ranvier nodes. *Pflügers Arch.* **309**, 176–192.

NONNER, W. (1979). Does immobilization of 'gating' charge reflect properties of Na inactivation in myelinated nerve? *Biophys. J.* **25**, 194*a*.

NONNER, W., ROJAS, E. & STÄMPFLI, R. (1975). Gating currents in the node of Ranvier: voltage and time dependence. *Phil. Trans. R. Soc.* B **270**, 483–492.

NONNER, W., ROJAS, E. & STÄMPFLI, R. (1978). Asymmetrical displacement current in the membrane of frog myelinated nerve: early time course and effects of membrane potential. *Pflügers Arch.* **375**, 75–85.

SIGWORTH, F. J. (1977). Sodium channels in nerve apparently have two conductance states *Nature, Lond.* **260**. 265–267.